Noname manuscript No.
(will be inserted by the editor)

Effect of spatial inhomogeneities on detonation propagation with yielding confinement

X.C. Mi · A.J. Higgins · C.B. Kiyanda · H.D. Ng · N. Nikiforakis

Received: date / Accepted: date

Abstract The propagation of detonation in layers of reactive gas bounded by inert gas is simulated computationally in both homogeneous and inhomogeneous systems described by the two-dimensional Euler equations with the energy release governed by an Arrhenius rate equation. The thickness of the layer is varied and the detonation velocity is recorded as the layer thickness approaches the critical value necessary for successful propagation. In homogeneous systems, as activation energy is increased, the detonation wave exhibits increasingly irregular cellular structure characteristic of the inherent multidimensional instability. The critical layer thickness necessary to observe successful propagation increases rapidly, by a factor of five, as the activation energy is increased from $E_a/RT_0 = 20$ to 30; propagation could not be observed at higher activation energies due to computational limitations. For simulations of inhomogeneous systems, the source energy is concentrated into randomly positioned squares of reactive medium embedded in inert gas; this discretization is done in such a way that the average energy content and the theoretical Chapman-Jouguet (CJ) speed remains the same. In the limit of highly discrete systems with layer thicknesses much greater than critical, velocities greater than the CJ speed are obtained, consistent with our prior results in effectively infinite width systems. In the limit of highly discretized systems wherein energy is concentrated into pockets representing 10% or less of the area of the reactive layer, the detonation is able to propagate in layers much thinner (by an order of magnitude) than the equivalent homogenous system. The critical layer thickness increases only gradually as the activation energy is increased from $E_a/RT_0 = 20$ to 55, a behavior that is in sharp contrast to the homogeneous simulations. The dependence of the detonation velocity on layer thickness and the critical layer thickness are remarkably well described by a front curvature model derived from the classic, ZND-based model of Wood and Kirkwood. The results of discrete sources are discussed as a conceptual link to the behavior that is experimentally observed in cellular detonations with highly irregular cellular structure in which intense turbulent burning rapidly consumes detached pockets behind the main shock front. The fact that highly discrete systems are well described by classical, curvature-based mechanisms is offered as a possible explanation as to why curvature-based models are successful in describing heterogeneous, condensed phase explosives.

Keywords Detonation · propagation limit · yielding confinement · flow divergence · losses · activation energy · inhomogeneous · critical phenomenon

X.C. Mi, A.J. Higgins
Department of Mechanical Engineering, McGill University, Montreal, Quebec, Canada H3A 0C3
E-mail: xiaocheng.mi@mail.mcgill.ca

C.B. Kiyanda, H.D. Ng
Department of Mechanical and Industrial Engineering, Concordia University, Montreal, Quebec, Canada H4B 1R6

N. Nikiforakis
Cavendish Laboratory, Department of Physics, University of Cambridge, Cambridge, United Kingdom CB3 0HE

1 Introduction

Among the various attempts to elucidate the complex dynamics of gaseous detonation waves over the past six decades, studies that probe the response of detonations to losses resulting from lateral divergence in the reaction zone perhaps have proven to be the most productive. By measuring how the detonation velocity decreases with increasing lateral losses and eventually

fails, the sensitivity of the energy release mechanism to losses can be revealed. This competition between release of chemical energy that sustains the wave and the losses due to flow expansion that result in its decline and failure lies at the heart of most critical phenomena in detonation. A key question these studies can ask is: Are detonations in systems characterized by highly irregular cellular structures—associated with large activation energies governing their reaction zone structure—more robust in their ability to continue propagation in the presence of losses in comparison to more regular mixtures associated with lower activation energies? Contradictory answers have been found as this problem has been approached from different angles.

Theoretical models of detonations with divergent flow that are based on a steady, quasi-one-dimensional solution (known as ZND-based models) assume a laminar-like wave structure and examine the reactive flow along the centerline with radial expansion [1–4]. These models exhibit a critical turning point in the relationship between the deficit in propagation velocity from the ideal Chapman-Jouguet (CJ) value and the loss parameter (in this case, flow divergence or the related curvature of the detonation front), and this critical point is associated with failure of the wave. Further analysis based on this type of model associates the detonation velocity vs. loss parameter relation with the effective activation energy governing the reaction process: A greater activation energy results in the detonation failing at velocities closer to the CJ velocity and smaller values of the loss parameter, so that detonations governed by high activation energies should be less resilient to losses.

Mounting experimental evidence has shown that, in contradiction to the predictions of ZND-based models described above, detonations that are characterized by highly irregular structures are able to continue to propagate at lower velocities while subjected to greater losses. In the experimental studies of detonations with mass divergence due to porous confinement, Radulescu and Lee have shown that highly irregular mixtures (i.e., propane-oxygen and methane-oxygen mixtures) result in detonation failure at significantly smaller tube diameters (normalized by the corresponding ZND induction zone length) than the critical tube diameters at which weakly unstable, argon-diluted detonations fail, which contradicts the predictions of the corresponding ZND-based model [5,6]. Recently, Borzou and Radulescu conducted experiments of detonations propagating in horn-shaped channels with a constant area divergence and found that detonations in highly unstable, propane-oxygen mixtures are able to propagate with a greater magnitude of area divergence (hence, greater losses) than those in weakly unstable, argon-diluted acetylene-oxygen mixtures [7]. By fitting their experimental results for the highly unstable mixtures to the ZND-based theoretical framework, Borzou and Radulescu determined an effective activation energy that is 70% lower than the value derived from detail chemical kinetics [7]. This inconsistency between theoretical predictions and experimental results is hypothesized to result from the fact that the classical, laminar-like picture of ZND-based models fails to describe the multidimensional and transient structure of real gaseous detonations.

Numerical simulations have enabled researchers to capture some of the multidimensional features of cellular detonations since the early 1980s [8,9] and hence have been used to seek further insights into detonation dynamics by attempting to resolve these features. Few computational studies, however, have explored critical phenomena at the boundary between when detonations can and cannot propagate in the presence of losses. A study exploring the effect of activation energy on cellular detonations responding to losses due to compressible confinement has recently been performed by Reynaud *et al.* [10] These authors, by solving the two-dimensional, reactive Euler equations, demonstrated that, as activation energy is increased, the critical reactive layer thickness (normalized by the corresponding ZND half-reaction-zone length) increases and the maximum velocity deficit decreases, suggesting a decrease in resistance to losses for increasingly unstable detonations [10, 11]. This result is qualitatively consistent with the predictions of the ZND-based model, however, it is in contradiction to experimental findings. It is important to note that, although the morphological features of the leading shock complex are captured in inviscid flow (Euler-based) simulations, the turbulent-driven mechanism governing the burnout of the large pockets of weakly shocked reactant in cellular detonations cannot be accurately described by such simulation. Burning via turbulent-driven mixing in real detonations has been conjectured to be able to more effectively release the energy contained in these weakly shocked pockets [12,13, 7,14], and thus facilitate the propagation of highly unstable detonations wherein these pockets may contain as much as half of the gas processed by the wave [15–18]. As validated turbulent burning models at the reaction zone conditions of real gaseous detonations are still under development, and direct numerical simulation of three-dimensional, reactive, compressible turbulence is likely beyond computational capacity for the coming decade, different approaches to modeling this problem are necessary in the meantime.

Recently, a different approach to the detonation dynamics problem has been proposed by the present au-

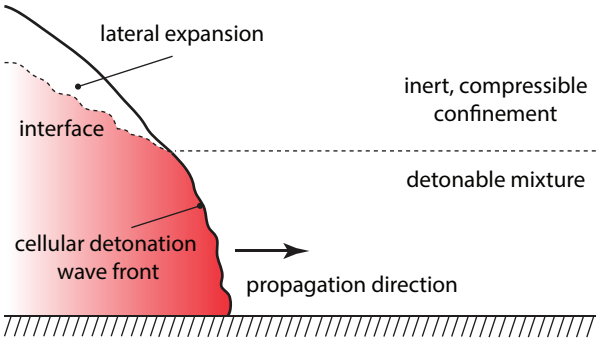

Fig. 1 Conceptual illustration of a cellular detonation wave propagating in a detonable mixture of gases confined by an inert gas layer.

thors in considering the influence of concentrating the energy release into reactive pockets embedded in an otherwise inert media [19–22]. Conceptually, this corresponds to an inhomogeneous detonable mixture resulting from incomplete mixing, a problem with some relevance to propulsion and explosion safety (discussed below), but more generally, this approach attempts to study the influence that spatially localized reaction centers, such as those that arise spontaneously in unstable, cellular detonations, have on detonation dynamics. This picture of detonation as propagating via random reaction centers also has some conceptual similarity to hot spots in condensed-phase explosives and may inform our understanding of detonation in such media. The premise of this approach is that examining the influence of spatially concentrated reaction centers may enable fully computationally resolved simulations to be conducted, reflecting some element of the dynamics that occur in highly irregular cellular detonations that at present cannot be resolved. Examination of this discrete source approach in systems without losses has already revealed some unusual results: As the energetic content of a medium is collected into sufficiently concentrated pockets, the average wave velocity of the detonation propagating through the system may be as much as 15% greater than the CJ speed of the equivalent homogeneous system due to the highly non-equilibrium nature of the flow at the effective sonic point [20–22].

In the present paper, the approach of imposing spatially discretized sources will be extended to a two-dimensional system of a detonable gaseous mixture confined by an inert gas layer. The problem of a detonation in a reactive layer with yielding confinement (as illustrated in Fig. 1) is particularly convenient for studying the dynamics for a number of reasons: (i) The base flowfield is quasi-steady (unlike the unsteady direct initiation or critical diameter problems), (ii) resolving the details of a wall-interaction viscous boundary layer is not required (as is necessary for detonations in narrow tubes and channels), and (iii) in the limit as the reactive layer becomes very large, the classical CJ detonation velocity is usually recovered, providing a well-defined asymptotic limit.

The problem of a detonation propagating in a layer or column of detonable mixture surrounded by an inert gas has been studied experimentally since the 1960s [23–25]. Initially, this problem was motivated as a gas-phase analog to a cylindrical rate-stick experiment, the standard test used to quantify conventional high explosives. Concerning the relevance to industrial accident scenarios, researchers have revisited this problem with their focus upon linking critical layer dimensions for a self-sustained propagation to other dynamic parameters of detonations, such as detonation cell size and the critical diameter for a transition to unconfined detonation [26–33]. Much recent interest in the problem of a detonation propagating in thin reactive layers bounded by non-reacting gas—and in layers with spatially inhomogeneous reactive composition—has been motivated by the rotating detonation engine (RDE) concept [10, 34–37]. The detonable layer in an RDE is bounded by the combustion products (residual from the prior cycle) on one side of the wave, and the dynamics of detonation propagation in this layer is crucial to the operation of the engine. In most embodiments, the fuel and oxidizer are injected separately to avoid detonation-driven flashback into a mixing chamber, resulting in significant non-uniformities in the detonable mixture. In some recent studies, numerical simulations of detonation waves in RDE-relevant combustion scenarios result in super-CJ propagation with discretely spaced fuel-oxidizer injection [38,39].

In this study, the inhomogeneities are introduced as a spatially random distribution of discrete, reactive pockets in the detonation system with inert, yielding confinement. Numerical simulations based on the two-dimensional, reactive Euler equations are performed for both homogeneous and randomly inhomogeneous cases, and the results are compared to a ZND-type model that assumes the front is governed by a globally curved and laminar-like structure. The objective of this paper is to examine the influence of the characteristics of the imposed spatial inhomogeneity and the governing activation energies on the near-limit wave propagation, specifically addressing the question: What is the comparative influence on the critical layer thickness of activation energy and spatial discreteness?

This paper is organized as follows. In Sect. 2, the problem considered in the simulations is stated. Section 3 describes the numerical methodology used to solve the governing equations. The simulation results of wave structures, the history of instantaneous prop-

agation speed, the averaged propagation speed as a function of the reciprocal of the reactive layer thickness $1/h$, and the critical thickness for self-sustained propagation h^* as a function of spatial discreteness Γ and activation energy E_a are presented in Sect. 4. The results are also compared to a curvature-based model that assumes a ZND-like structure of the detonation. The findings based upon the simulation results are discussed in Sect. 5 and summarized in the Conclusions (Sect. 6). Numerical convergence tests performed for selected simulation results are reported in the Appendix.

2 Problem statement

The reactive system consists of an inviscid, calorically perfect gas (i.e., with a constant ratio of specific heat γ). The gasdynamics of this system is described by the two-dimensional reactive Euler equations in a lab-fixed reference frame with flow and state variables non-dimensionalized with respect to the pre-shock, initial state. The governing equations are formulated as follows,

$$\frac{\partial \mathbf{U}}{\partial t} + \frac{\partial \mathbf{F}\left(\mathbf{U}\right)}{\partial x} + \frac{\partial \mathbf{G}\left(\mathbf{U}\right)}{\partial y} = \mathbf{S}\left(\mathbf{U}\right) \tag{1}$$

where the conserved variable $\mathbf{U}$, the convective fluxes $\mathbf{F}$ and $\mathbf{G}$, and reactive source term $\mathbf{S}$ are, respectively,

$$\mathbf{U} = \begin{pmatrix} \rho \\ \rho u \\ \rho v \\ \rho e \\ \rho Z \end{pmatrix} \qquad \mathbf{F} = \begin{pmatrix} \rho u \\ \rho u^2 + p \\ \rho uv \\ (\rho e + p)u \\ \rho Z u \end{pmatrix}$$

$$\mathbf{G} = \begin{pmatrix} \rho v \\ \rho uv \\ \rho v^2 + p \\ (\rho e + p)v \\ \rho Z v \end{pmatrix} \qquad \mathbf{S} = \begin{pmatrix} 0 \\ 0 \\ 0 \\ 0 \\ \rho \Omega \end{pmatrix} \tag{2}$$

In the above equations, e is the non-dimensional specific total energy, and Z is the reaction progress variable, or the normalized concentration of reactant, which varies between 1 (unreacted) and 0 (fully reacted). For a homogeneous reactive system, the specific total energy is defined as $e = p/(\gamma - 1)\rho + (u^2 + v^2)/2 + ZQ$. In this study, the reaction rate $\Omega = \partial Z/\partial t$ is governed by single-step Arrhenius chemical kinetics as follows,

$$\Omega = -kZ \exp\left(-E_\mathrm{a}/T\right) \tag{3}$$

where k and E_a are the dimensionless pre-exponential factor and activation energy, respectively. Note that the activation energy is non-dimensionalized with respect to the initial, pre-shock thermodynamic state, i.e., $E_\mathrm{a} = \widetilde{E_\mathrm{a}} / \left(\widetilde{R}\widetilde{T_0}\right)$ (where the tilde "$\sim$" denotes a dimensional quantity), not with respect to the corresponding von Neumann state. Specific values were selected for the preexponential factor k so that the half-reaction-zone length $l_{1/2}$ in the ideal ZND solution for the homogeneous case with the corresponding E_a equals to unity. Thus, all the length quantities reported in this paper are in the unit of the corresponding $l_{1/2}$.

The initial configuration of the simulation system is illustrated in Fig. 2(a). The red region on the bottom is the reactive gas layer with a thickness h; the blue region on the top is the inert gas layer with a thickness h_I, where Z equals 0 initially. The critical thickness of the reactive layer below which a detonation wave fails to propagate is denoted as h^* in this paper. A high-pressure region near the left end of the simulation domain, as shown in Fig. 2(a), is used to initiate a rightward-propagating detonation wave. For the cases with a low activation energy, i.e., $E_\mathrm{a} = 10$, 20, and 25, the pressure and density in the initiation zone was set equal to twice the corresponding CJ state properties, i.e., $p = 2p_\mathrm{CJ}$ and $\rho = 2\rho_\mathrm{CJ}$; for the cases with a relatively high activation energy, i.e., $E_\mathrm{a} \geq 30$, the pressure and density in the initiation zone were set to $p = 5p_\mathrm{CJ}$ and $\rho = 2\rho_\mathrm{CJ}$. Two different amounts of initiation energy were used for cases with low and high activation energies to ensure that the detonation wave can be successfully initiated while minimizing the overdriving effect. The rest of the simulation domain was initialized with uniform, density, and particle velocity as $p = 1$, $\rho = 1$, $u = 0$, and $v = 0$.

The spatial inhomogeneities were introduced to the simulation system as spatially discrete reactive squares, similar to those in previous studies where this approach of imposing discrete sources were first proposed [20,21]. The reaction progress variable Z was initialized as 1 in these reactive sources and 0 in the inert regions separating them. Different from a regularly spaced array of sources introduced in Ref [21], square sources of the same size were randomly assigned in the reactive layer. With a prescribed average spacing between neighboring sources L, the spatial discreteness parameter Γ can be defined as the ratio between the size of a source and the inert area surrounding it, i.e., $\Gamma = W^2/L^2$. In the limit of $\Gamma \to 1$, the reactive layer becomes homogeneous where the initial distribution of Z is uniform; in the limit of $\Gamma \to 0$, a discrete source approaches a δ-function in space, namely, a point source of energy. In order to maintain the average specific energy release Q the same as that in the homogeneous cases, the energy release associated with each discrete

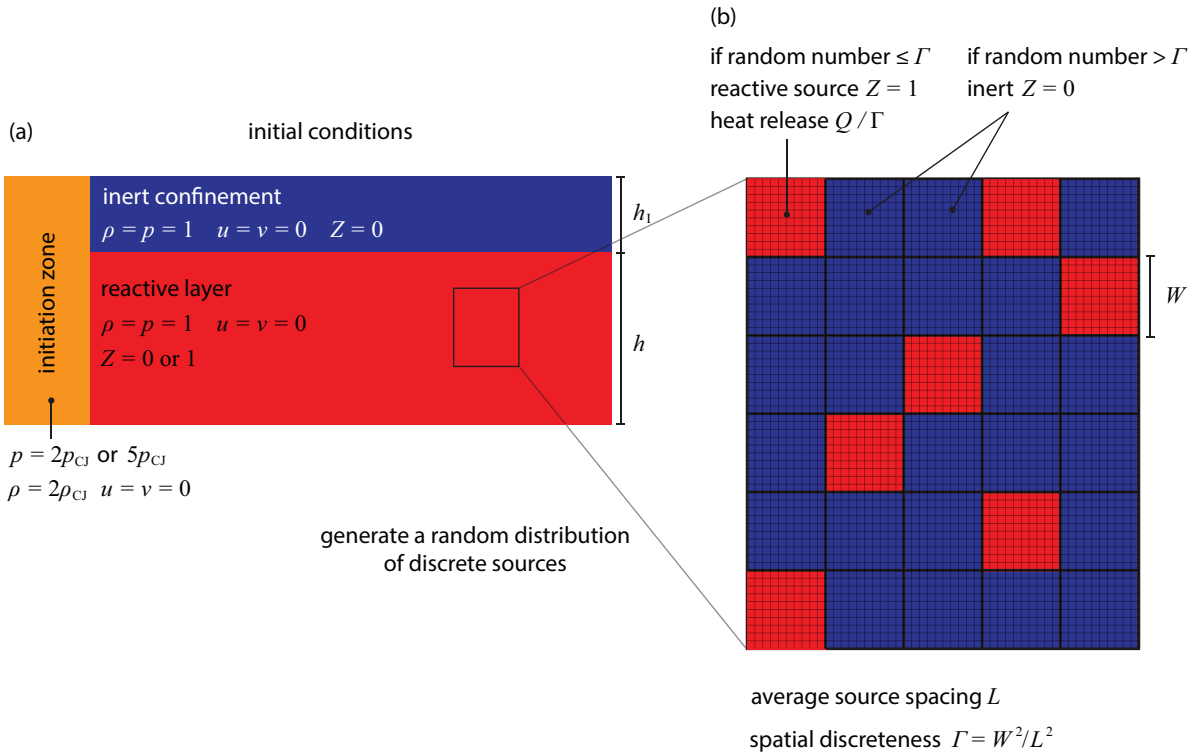

Fig. 2 Schematic illustration of (a) the initial conditions for the simulation system and (b) the method used to initialize a spatially random distribution of discrete sources.

source must be increased according to the prescribed spatial discreteness Γ. For the cases with spatial inhomogeneities, the specific total energy is formulated as $e = p/(\gamma-1)\rho + (u^2+v^2)/2 + ZQ/\Gamma$. The method used to randomize the positions of the discrete sources while maintaining a prescribed value of the overall discreteness Γ is described in the next section.

3 Numerical methodology

The simulation code used to solve the two-dimensional reactive Euler equations is based upon a uniform Cartesian grid. The MUSCL-Hancock scheme with the van Leer nonsmooth slope limiter and a Harten-Lax-van Leer-contact (HLLC) approximate solver for the Riemann problem was used [40]. This code is implemented in Nvidia's CUDA programming language [41,42]. The simulations were performed on a Nvidia Tesla K40M and P100 GPU computing processors. The Strang splitting method was adopted to treat separately the hydrodynamic process and the reactive process. This numerical scheme is thus of second-order accuracy in space and time.

In each case where a detonation wave successfully propagated, the length (in x-direction) of the entire simulation domain was approximately 3000 times the half-reaction-zone length $l_{1/2}$ for an ideal, homogeneous case. The technique of an advancing computational window, which was developed in several recent studies for simulating detonation waves propagating over a long distance [43–45,10], was used in this study in order to reduce the computational cost. Instead of the entire domain, the simulations were only performed in a window that enclosed the leading wave complex. Two window sizes, $600l_{1/2}$ and $400l_{1/2}$ in the wave propagation direction, were used in this study. The smaller window size was used when the width of the computational domain in the transverse direction was large, i.e., for larger reactive layer thickness h. Once the leading shock front nearly reached the end of the computational window (i.e., $20l_{1/2}$ away from the right boundary along the bottom boundary), the left and right boundaries of the window were advanced by either half or quarter of the window size, $600l_{1/2}$ or $400l_{1/2}$, respectively, thus ensuring a distance of approximately $300l_{1/2}$ between the leading wave front and the rear (left) boundary. This distance was verified to be sufficiently large to capture the reaction zone dynamics that contribute to the propagating wave front. In addition, this technique of an advancing computational window ensures that any long term initiation-zone influence on the steady-state wave propagation is eliminated.

On the top, left, and right boundaries of this computational window, a transmissive, outflow boundary condition was implemented. The ghost cells took the lowest-order extrapolation of the values in the adjacent cells as explained by Oran and Boris.[46] It has been shown buy Kasimov and Stewart that the use of transmissive boundary condition can result in non-physical waves being reflected into the computational domain.[47] Therefore, for all simulations reported in this paper, a minimum thickness of the inert layer $h_{\mathrm{I}} = 50l_{1/2}$ (i.e., a thickness of 500 computational grid for a resolution of $l_{1/2}/\Delta x = 10$) was used to ensure that any reflected waves from of the top boundary would not influence the propagation dynamics.

On the bottom boundary, a reflecting boundary is applied to model a rigid confining wall or plane of symmetry. This boundary condition enforces zero normal velocity, and flow can move freely in the tangential direction to the bottom boundary. Thus, there is no influence of diffusivity and viscosity due to this boundary condition. For the cases with an infinitely large reactive layer, the entire simulation domain with a width (in y-direction) of $300l_{1/2}$ is initialized as a reactive medium; periodic boundary conditions are applied in the top and bottom boundaries.

As the average source spacing L and the overall spatial discreteness Γ were prescribed, the width of each square source W was calculated as $W = \sqrt{\Gamma L^2}$. In order to initialize the simulation domain with a spatially random distribution of discrete sources, the reactive layer was first divided into squares of a size W^2 as marked by the thick black lines in Fig. 2(b). Note that a source-sized square is much larger than the size of the computational cells shown as gray lines. A random number N_{r} between 0 and 1 was assigned to each source-sized square using a uniform random number generator. As shown in Fig. 2(b), if a N_{r} is less than or equal to the spatial discreteness Γ, a reactive source is placed at this square, and all the computational cells within this square are initialized with $Z = 1$; otherwise, the square contains only inert material with $Z = 0$. A numerical resolution of 10 computational cells per half-reaction-zone length of the ideal homogeneous case, i.e., $l_{1/2}/\Delta x = 10$, was for most of the simulations reported in this paper. For selected cases, simulations were performed at different resolutions, i.e., $l_{1/2}/\Delta x = 5$, 20, and 30, for convergence tests. For the cases with very small discrete sources, e.g., $W = 1$ corresponding to $L = 10$ and $\Gamma = 0.01$, the minimum resolution ensures a sufficient number of computational cells within a square source (100 cells in the source with 10 cells along each side of the square). A complete study of grid resolution is reported in the Appendix.

4 Results

For all the simulations performed in this paper, the average specific energy release $Q = 50$ and the ratio of specific heats $\gamma = 1.2$ were selected to represent a typical detonate mixture of gases. The selected $Q = 50$ and $\gamma = 1.2$ are canonical values that have been extensively studied in the literature of gaseous detonations.[48–53, 47,54,55] In order to examine the effect of various activation energies, four different values of E_{a}, i.e., $E_{\mathrm{a}} = 10$, 20, 25, and 30, were considered for both homogeneous and inhomogeneous cases; two larger activation energies, $E_{\mathrm{a}} = 40$ and 55, were considered only for highly inhomogeneous cases with $\Gamma = 0.01$. The average source spacing L and the spatial discreteness Γ were independently varied to quantitatively control the nature of the imposed spatial inhomogeneities. For each set of simulations with fixed E_{a}, L, and Γ, the only variable parameter is the thickness of the detonable layer h. Some selected results showing the wave structure for both homogeneous and inhomogeneous cases with various governing parameters are presented in Sect. 4.1. Sample plots of the propagation velocity histories resulting from different cases, which allows one to identify whether a detonation wave successfully propagates or not, are shown in Sect. 4.2. The measured average propagation velocity V_{avg} for all the cases considered in this study plotted as functions of the reciprocal of the detonable layer thickness, i.e., $1/h$, and the determined critical thickness h^* below which a detonation wave extinguishes are summarized in Sect. 4.3 and 4.4, respectively.

4.1 Wave structure

Sample wave structures shown in Fig. 3 are for the case of a low activation energy $E_{\mathrm{a}} = 10$. The top half of each subfigure is the contour plot of reaction progress variable Z; the bottom half is the contour plot of pressure. The red area in the plot of Z is the reactive regions, or discrete sources in the inhomogeneous cases (Fig. 3(b) and (c)). The white dash lines indicate the interface between the reactive medium and the inert confinement. With a homogeneous reactive medium, as shown in Fig. 3(a), the resulting wave front exhibits a nearly smooth curvature without any noticeable transverse waves. According to the linear stability analysis, for the cases with $E_{\mathrm{a}} = 10$, transverse instabilities may be present if the computational grid is further refined.[50,56] Such transverse waves are weak, near-acoustic waves with likely little influence on the leading wave front. Discretizing the reactive medium into square sources with $\Gamma = 0.25$ and an average source

spacing $L = 10$, significantly larger than the intrinsic reaction-zone length for an ideal, homogeneous case, the wave structure becomes irregular as shown in Fig. 3(b). A localized high-pressure region can be observed near the leading shock front. While fixing the spatial discreteness $\Gamma = 0.25$ and reducing the average source spacing to $L = 1$, i.e., equal to the $l_{1/2}$ for the ideal ZND solution, a slightly roughened wave front with an identifiable global curvature is recovered as shown in Fig. 3(c).

For $E_a = 20$, selected snapshots of the wave structures resulting from a homogeneous case and inhomogeneous cases with moderately discretized ($L = 10$, $\Gamma = 0.25$) and highly discretized ($L = 10$, $\Gamma = 0.01$) sources are shown in Fig. 4(a), (b), and (c), respectively. At the selected reactive layer thickness $h = 100$, a detonation wave can propagate in all three cases. In the homogeneous case (Fig. 4(a)), transverse waves interacting with a globally curved leading shock front can be observed. A thin blue-green streak attached to the confinement interface can be seen on the Z-plot in Fig. 4(a), indicating that flow behind the leading shock laterally expands and some partially reacted gas moves away from the detonation complex. For the case with moderately discrete sources ($L = 10$, $\Gamma = 0.25$), as shown in Fig. 4(b), the resulting reaction-zone wave structure appears to be spatially more inhomogeneous than that from an initially homogeneous medium, featuring spatially localized high-pressure pockets near the leading shock front. A global curvature of the leading shock front can still be identified. While maintaining a constant source spacing $L = 10$, decreasing Γ to 0.01 makes the chemical energy possessed by the medium highly concentrated into the small ($W = 1$) discrete sources as shown in Fig. 4(c). The resulting localized high-pressure pockets behind the leading shock are separated by rather large low-pressure regions. Although the shock front propagating in the reactive layer can be distinguished from the oblique shock compressing the inert confinement, it does not seem to exhibit a globally curved shape.

4.2 Velocity history

For each simulation run, the trajectory of the leading shock front $x_s(t)$ along the rigid wall (the bottom boundary of the simulation domain) can be recorded by finding the location where pressure increases to $p = 1.01$ from its initial value $p = 1$ every unity time step. The instantaneous propagation velocity V can then be calculated by numerically differentiating $x_s(t)$ over time. For some selected cases with $E_a = 20$, sample results of the instantaneous propagation velocity histories normalized by V_{CJ} as a function of the leading shock position are plotted in Fig. 5.

As shown in Fig. 5(a) and (b), for both homogeneous and inhomogeneous ($L = 10$ and $\Gamma = 0.25$) cases, respectively, with a reactive layer thickness $h = 80$, the detonation wave can self-sustainably propagate. The fluctuation in V for the homogeneous case shown in Fig. 5(a) has an average amplitude of approximately 80% of V_{CJ} (from 0.6 to $1.4V_{CJ}$). For the inhomogeneous cases with $h = 80$ (Fig. 5(b)), V fluctuates over a much larger range from 0.5 to $1.8V_{CJ}$. The inhomogeneous case shown in Fig. 5(c) has a much thinner reactive layer of $h = 40$. The resulting velocity history exhibits some fluctuations around V_{CJ} after the initiation process, and decreases to a very low value (below $0.2V_{CJ}$). A velocity history as shown in Fig. 5(c) indicates that a detonation wave cannot successfully propagate at this reactive layer thickness, i.e., $h < h^*$, for the given set of parameters.

4.3 Average velocity

4.3.1 Results of the simulations

For a case of simulation where the resulting detonation wave successfully propagates, although the instantaneous propagation velocity exhibits fluctuations due to the presence of inhomogeneities in energy release, a quasi-steady propagation velocity can be measured in an average sense over time or propagation distance. The total distance over which a detonation wave propagates in such a simulation run is approximately 3000. The average propagation velocity V_{avg} is measured over the second half of the propagation distance, i.e., from $x_s \approx 1500$ to 3000, in order to avoid the influence of the initiation process on the measurement. The measured values of V_{avg} normalized by the CJ velocity are plotted as a function of the reciprocal of the reactive layer thickness $1/h$ for the cases with $E_a = 10$, 20, and 30 in Fig. 6(a), (b), and (c), respectively. The results are plotted as a function of the reciprocal of the layer thickness so that extrapolation to the y-axis corresponds to the infinite thickness layer case. Two average velocities over smaller distances, i.e., $x_s \approx 1500$ to 2250 and $x_s \approx 2250$ to 3000, are also measured to provide information regarding the uncertainty in the measurement of V_{avg} and plotted as error bars on the data points in Fig. 6.

The results plotted in Fig. 6(a) are for the cases with a very low activation energy $E_a = 10$. As the reactive layer thickness decreases (i.e., $1/h$ increases), the average velocity resulting from homogeneous and inhomogeneous cases decreases. The V_{avg} for the inhomoge-

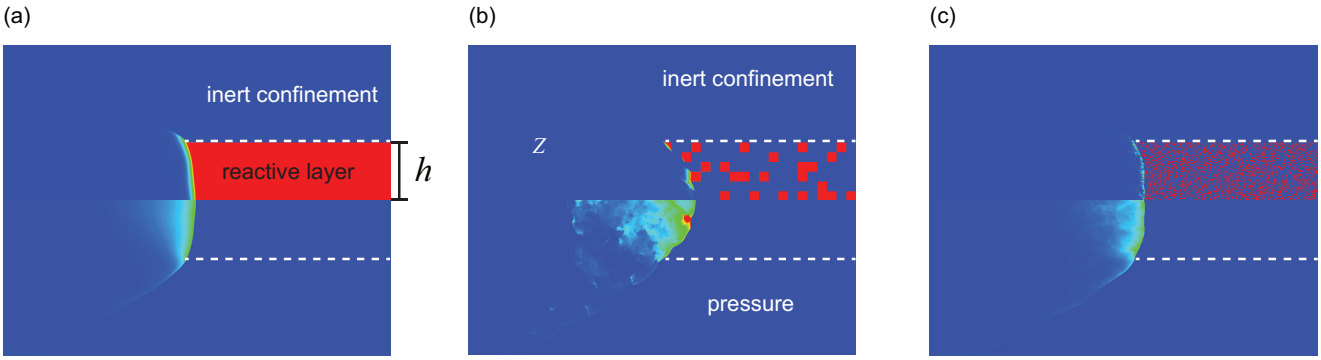

Fig. 3 Wave structures (contour plots of reaction progress variable on top and pressure on bottom) for the cases with $E_a = 10$, $h = 30$, and (a) a spatially homogeneous reactive medium, (b) an inhomogeneous medium with discrete sources of $L = 10$, $\Gamma = 0.25$ and (c) $L = 1$, $\Gamma = 0.25$.

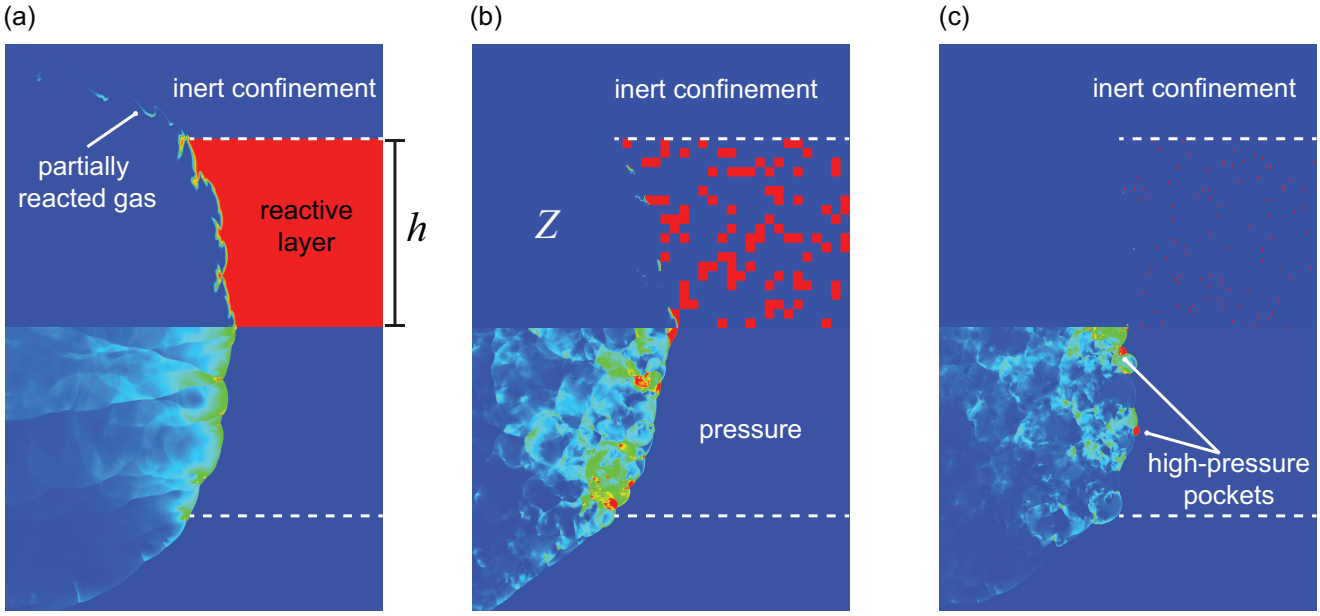

Fig. 4 Wave structures (contour plots of reaction progress variable on top and pressure on bottom) for the cases with $E_a = 20$, $h = 100$, and (a) a spatially homogeneous reactive medium, (b) an inhomogeneous medium with moderately discrete sources ($L = 10$, $\Gamma = 0.25$), and (c) an inhomogeneous medium with highly discrete sources ($L = 10$, $\Gamma = 0.01$).

neous cases with an average source spacing $L = 10$ (red circles) are slightly greater than those resulting from the homogeneous cases (blue squares). For the inhomogeneous cases with an average source spacing $L = 1$ (green diamonds), the resulting V_{avg} are very close to those for the homogeneous cases. For all three of these cases, the resulting V_{avg} decreases with h in a seemingly linear fashion; no case resulting in a quenched detonation was obtained for this low activation energy $E_a = 10$.

In Fig. 6(b) and (c), the results of V_{avg}/V_{CJ} are plotted as a function of $1/h$ for the cases with relatively higher activation energies, i.e., $E_a = 20$ and $E_a = 30$. A thin blue curve is plotted through the data for the homogeneous cases in both Fig. 6(b) and (c) to visually indicate the V_{avg}/V_{CJ} vs. $1/h$ trend; a vertical dash line is plotted to indicate the critical thickness marking the propagation limit. For an infinitely large reactive medium (realized by applying periodic boundary condition on the top and bottom boundaries of the domain), i.e., an adiabatic detonation system without losses, the V_{avg} resulting from the homogeneous cases with both $E_a = 20$ and 30 is very close to V_{CJ} (with less than 1% difference). As the reactive layer thickness decreases, the velocity deficit from the CJ value becomes greater until the propagation limit is encountered.

For the cases with $E_a = 20$ and moderately discretized sources ($\Gamma = 0.25$, red circles in Fig. 6(b)), the resulting V_{avg} is not significantly different from that of the homogeneous cases at large reactive layer thicknesses (small $1/h$). Approaching to the critical thickness, the V_{avg} for the $\Gamma = 0.25$ inhomogeneous be-

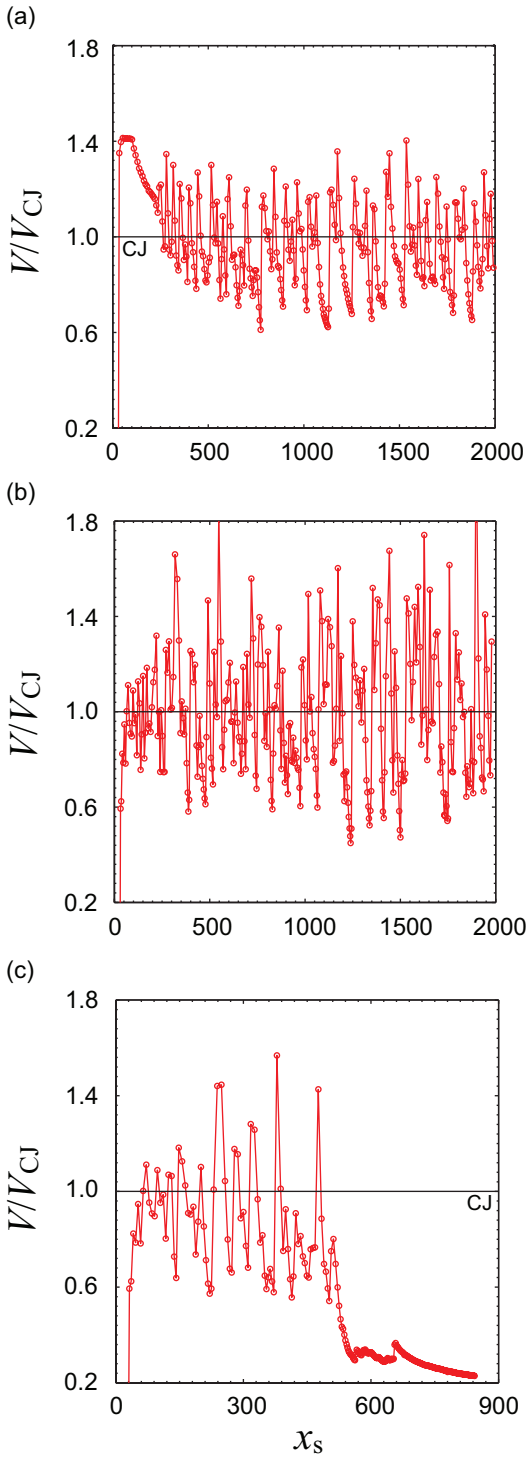

Fig. 5 The history of instantaneous propagation velocity V normalized by the Chapman-Jouguet (CJ) velocity V_{CJ} as a function of the leading shock position x_s for $E_a = 20$: (a) a homogeneous case with $h = 80$; inhomogeneous cases ($L = 10$ and $\Gamma = 0.25$) with (b) $h = 80$ and (c) $h = 40$.

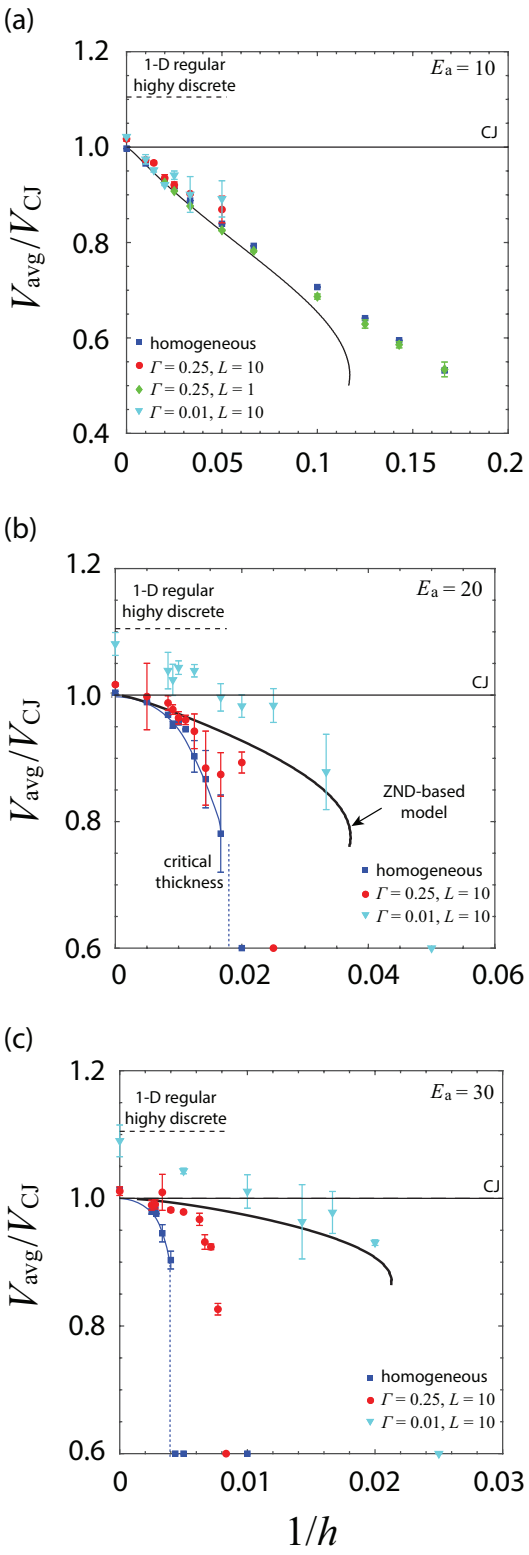

Fig. 6 Average propagation velocity V_{avg} normalized by the CJ velocity as a function of the reciprocal of the reactive layer thickness $1/h$ for the cases with (a) $E_a = 10$, (b) $E_a = 20$, and (c) $E_a = 30$. The black curve on each plot is the theoretical prediction using the Wood and Kirkwood model with a curvature-based geometric construction of the wave front.

comes significantly greater than that for the homogeneous cases. For the cases with highly discretized reactive sources ($\Gamma = 0.01$, cyan downward-pointing triangles in Fig. 6(b)), the resulting V_{avg} is significantly greater than the CJ velocity for the ideal, homogeneous system with the same amount of overall heat release at large reactive layer thicknesses. As shown in Fig. 6(b), the propagation limit for the cases with highly discretized sources ($\Gamma = 0.01$) is encountered at a much smaller critical thickness than that for the homogeneous cases.

For the cases with $E_{\text{a}} = 30$ as shown in Fig. 6(c), the homogeneous cases (blue squares) reaches the propagation limit at a larger h compared to those with an inhomogeneous medium. Making the reactive source sufficiently discrete, the resulting V_{avg} are significantly greater than V_{CJ} at relatively large reactive layer thickness. As Γ decreases from 0.25 (red circles) to $\Gamma = 0.01$ (cyan downward-pointing triangles), i.e., making the reactive medium increasingly discretized, a detonation wave can self-sustainably propagate into thinner reactive layers.

The horizontal dash-dotted lines added on Fig. 6(b) and (c) indicate the super-CJ propagation velocity as a result of a one-dimensional array of regularly spaced, highly discretized sources of energy for the case with $Q = 50$ and $\gamma = 1.2$. This result was obtained via numerical simulation and first reported in Ref. [20]. In the limit of extremely discretized sources ($\Gamma \to 0$), the resulting super-CJ velocity has been shown to be independent of the detail mechanism of energy deposition [20,21]. It is, hence, valid to compare the current results of V_{avg} with single-step Arrhenius kinetics to the result obtained in Ref. [20] where an instantaneous energy deposition was considered.

4.3.2 Model prediction

The prediction of the V_{avg} vs. $1/h$ relation using a theoretical model is plotted as the black curves in each subfigure of Fig. 6. This model is based on the assumption of a smoothly curved leading shock front followed by a steady, laminar-like reaction zone structure. First, using Wood and Kirkwood's quasi-one-dimensional model along the central streamline (equivalent to that along the rigid wall confinement in the problem considered in this study), the relation between the normal detonation velocity and the wave front curvature (D_{n}-κ relation), can be solved [1]. The smoothly curved leading wave front can then be geometrically constructed knowing the D_{n}-κ relation using the method first developed by Eyring *et al.* [57] This theoretical model, combining Wood and Kirkwood's solution and Eyring *et al.*'s geometric construction (see more details in Appendices of Refs. [45,22]), was used by Li *et al.*[45,44] to predict the V_{avg} vs. $1/h$ relation. As demonstrated by Li *et al.* [45], given the appropriate D_{n}-κ relation and shock angle at the confinement-explosive interface, the steady-state wave front constructed using Eyring *et al.*'s method is identical to those obtained using the Detonation Shock Dynamic model [58–60].

For the cases with a low activation energy $E_{\text{a}} = 10$ shown in Fig. 6(a), the theoretical prediction is very close to the simulation results for both homogeneous and inhomogeneous cases at large thicknesses; a propagation limit, marked by the turning point of the V_{avg} vs. $1/h$ curve, is predicted by this model, but it is not captured by the numerical simulations. For higher activation energies $E_{\text{a}} = 20$ and 30 shown in Fig. 6(b) and (c), respectively, the model predicts significantly smaller velocity deficits and critical reactive layer thickness than the simulation results for the homogeneous and moderately inhomogeneous ($\Gamma = 0.25$) cases. The simulation results of V_{avg} for the near-limit cases with highly discretized inhomogeneities ($\Gamma = 0.01$) appear to be fairly close to the turning point of the theoretical prediction curves in Fig. 6(b) and (c).

4.4 Critical thickness h^*

With values of activation energy $E_{\text{a}} \geq 20$, the failure of detonation propagation is captured in the cases with both a homogeneous reactive layer and a random distribution of discrete sources (as shown in Fig. 6(b) and (c) for $E_{\text{a}} = 20$ and 30, respectively. The critical thickness of the reactive layer h^* below which a detonation fails to propagate can thus be determined for these cases and summarized in Figs. 7 and 8. For each data point plotted on these two figures, the upper error bar indicates the smallest thickness at which the simulation results in a self-sustained propagation, h^*_{go}; the lower error indicates the largest thickness at which a failure of propagation is identified, $h^*_{\text{no-go}}$. The critical thickness h^* is determined as the average value between h^*_{go} and $h^*_{\text{no-go}}$, i.e., $h^* = (h^*_{\text{go}} + h^*_{\text{no-go}})/2$. In other words, the critical thickness h^* is bounded by h^*_{go} and $h^*_{\text{no-go}}$.

The simulation results of h^* are plotted as a function of Γ, the spatial discreteness of the imposed inhomogeneous sources, with a fixed average source spacing $L = 10$ in Fig. 7. On the right end of this plot, $\Gamma = 1$ is associated with the cases of a homogeneous reactive layer. The results with $E_{\text{a}} = 20$, plotted as circles, show that the critical thickness decreases from $h^* = 57.5 \pm 2.5$ to 25 ± 5 as the reactive medium is varied from spatially homogeneous to highly discretized, i.e., from $\Gamma = 1$ to $\Gamma = 0.01$. For the cases with $E_{\text{a}} = 30$, the resulting h^*

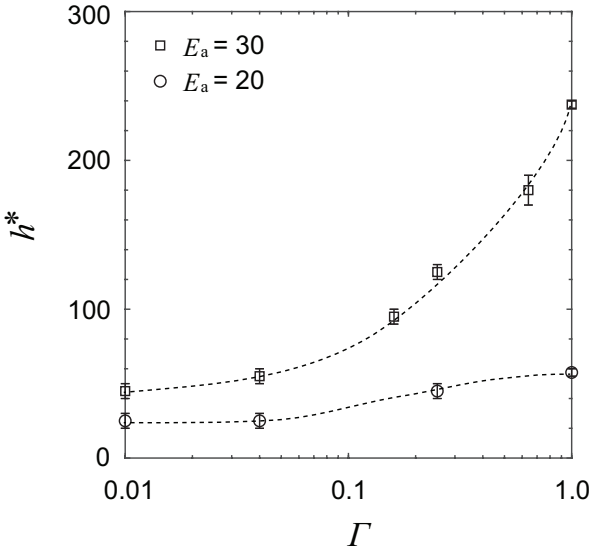

Fig. 7 Critical thickness of the reactive layer h^* as a function of spatial discreteness Γ for $E_a = 20$ (marked as circles) and $E_a = 30$ (marked as squares).

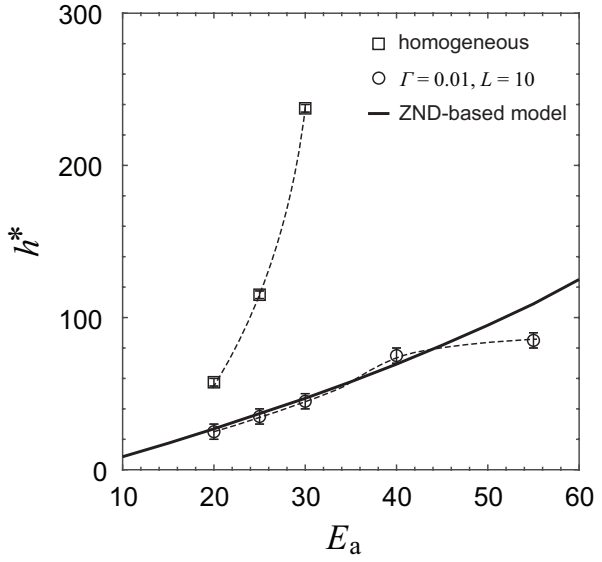

Fig. 8 Critical thickness of the reactive layer h^* as a function of activation energy E_a with a homogeneous medium (marked as squares) and with a highly inhomogeneous medium of $\Gamma = 0.01$ and $L = 10$ (marked as circles). The black curve is the theoretical prediction using the Wood and Kirkwood (ZND-based) model with a curvature-based geometric construction of the wave front.

(squares in Fig. 7) decreases from 247.5 ± 2.5 to 45 ± 5 as Γ decreases from $\Gamma = 1$ to $\Gamma = 0.01$, exhibiting a steeper slope of change with the spatial discreteness of the reactive medium than that associated with the $E_a = 20$ results. The simulation results shown in Fig. 7 are at a numerical resolution of 10 computational cells per the half-reaction-zone length ($l_{1/2}/\Delta x = 10$), which has been verified to be sufficient to obtain converged results of h^* (see Appendix).

In Fig. 8, the simulation results of critical thickness h^* as a function of activation energy E_a for the homogeneous $\Gamma = 1$ cases are plotted as square symbols. A dash line is drawn through the data point as a visual guide showing the trend of the results, not a numerically fitted function. The results of h^* for the homogeneous cases increases nearly fivefold (from 57.5 to 247.5) as E_a increases from 20 to 30. This result suggests that simulations for homogeneous media with greater activation energies $E_a > 30$ would require a larger domain size and greater numerical resolution ($l_{1/2}/\Delta x \geq 20$) to capture the critical thickness (as discussed in the Appendix). Therefore, performing those simulations is beyond the computational capacity that is available to the authors at this time, and thus no simulations of homogeneous media were conducted at $E_a > 30$.

The simulation results of h^* for the most highly discretized cases with $\Gamma = 0.01$ and $L = 10$ as a function of E_a are plotted as circles in Fig. 8. A dash line is added to show the trend of these data. The resulting h^* increases from 25 ± 5 to 85 ± 5, at a significantly lower rate comparing to the results for the homogeneous cases, as E_a increases from 20 to 55. The h^* vs. E_a relationship predicted by the ZND-based model (Wood and Kirkwood model with wave front construction) is plotted as the thick black curve in Fig. 8. This model prediction of h^* (that associates the turning points of the ZND-based model prediction curves plotted in Fig. 6) is significantly smaller than the results of the simulations for the homogeneous cases, however, appears to be very close to the simulation results for the highly inhomogeneous cases, especially for relatively low activation energies of $E_a < 40$.

5 Discussions

The simulation results reported in this paper show that the presence of discrete reactive sources significantly affects the propagation behaviour of detonations with yielding confinement as the sources become more spatially concentrated. In the cases with a reactive layer thickness that is significantly greater than the critical value, as shown in Fig. 6(b) and (c) for $E_a = 20$ and 30, respectively, the average propagation velocity increases beyond the CJ value for an increasingly discretized reactive medium, and tends to approach the super-CJ propagation speed obtained from one-dimensional simulations with regularly spaced, highly discretized sources of energy. This result is consistent with the results of our prior studies of detonations in discrete systems in domains with periodic boundary conditions (i.e., in the

absence of losses) [20–22]. Thus, the super-CJ V_{avg} results observed in the present study for highly inhomogeneous cases at large thicknesses can be interpreted as weak detonations due to the non-equilibrium state at the effective sonic surface, a hypothesis that has been further elucidated in Ref. [20–22].

We now turn to discuss the velocity deficit observed with lateral expansion of flow resulting from yielding confinement. For low values of activation energy, i.e., $E_{\text{a}} < 20$, the introduction of spatial concentration of energy release has little effect on detonation propagation, and detonation velocity deficits in both homogeneous and spatially discrete systems are well described by a front curvature model based on an assumed laminar, ZND-like structure. As the activation energy is increased to $E_{\text{a}} > 20$, a difference in behavior of the homogeneous and inhomogeneous systems is observed: a sufficiently inhomogeneous reactive media assists a detonation wave to propagate beyond the limit encountered in a homogeneous medium. For the cases with a relatively high $E_{\text{a}} = 30$, as varying the spatial inhomogeneity of the initial distribution of reactant from a homogeneous medium to highly discretized reactive sources, the critical thickness of the reactive layer for a self-sustained propagation is reduced by nearly an order of magnitude (as shown in Fig. 7). This sensitizing effect of spatial inhomogeneities on the near-limit propagation of detonation waves was first found by Li *et al.* [44] In their work, a pressure-dependent reaction model, which resulted in a smooth, laminar-like wave structure in the homogeneous case, was used, and the effect of introducing sinusoidal perturbations of the density and temperature fields was examined. The finding of this current study thus complements the work of Li *et al.* [44] by showing this sensitizing effect in an unstable detonable system governed by activated chemical kinetics. Given that the inhomogeneities were implemented as spatially concentrated reactant that could approach point-like sources in this study, a more pronounced effect of inhomogeneities on the propagation limit was found in the present study compared to that of Li *et al.* [44]

For the homogeneous cases, i.e., systems without imposed inhomogeneities, the simulation results of h^* increases by approximately a factor of five as activation energy increases from 20 to 30, results which are consistent with the findings reported by Reynaud *et al.* [10,11] that explored a range of $E_{\text{a}} = 10$–38.23 with $Q = 23.8$ and $\gamma = 1.33$. The qualitative trend of these results can likely be attributed to the shock strength (temperature) sensitivity of highly activated kinetics. As shown in Fig. 8, this increasing trend of h^* vs. E_{a} exhibited by the simulation results for the homogeneous cases is significantly steeper than that of the ZND-based model prediction.

In order to explain this quantitative discrepancy between simulation results and model prediction, some features of cellular detonations responding to yielding confinement that are captured by Euler-based simulations need to be considered. In the homogeneous cases, transverse waves, which originate from the perturbation caused by yielding confinement, develop themselves into a cellular wave structure. In such a cellular detonation complex, large pockets of reactive gas are processed by the leading shock at a strength that is considerably weaker than the corresponding CJ Mach number. The reaction within these weakly shock pockets is initiated at a relatively low temperature (much lower than the von Neumann temperature associated with M_{CJ}), and thus, progresses much more slowly. The overall strength of the leading shock complex decreases significantly due to lateral expansion in the transverse direction from the rigid wall towards the inert confinement. A more substantial amount of slowly reacting gas can thus be found near the expanding confinement interface downstream from the leading shock as indicated in Fig. 4(a). The energy release from these slowly reacting pockets of gas are unlikely to contribute to re-strengthening the leading shock wave. Hence, a near-limit, cellular detonation wave under yielding confinement suffers not only losses in momentum due to the lateral expansion, but also an insufficient support from the slow energy release of the weakly shocked reactant, especially near the reactant-confinement boundary. The mutually aggravating effect between these two mechanisms of losses might be responsible for this more dramatic decrease in detonation resilience to flow divergence that has been identified in Euler-based simulations with a homogenous medium.

As shown in Fig. 8, the h^* vs. E_{a} relationship obtained for the cases with highly discretized sources of energy ($\Gamma = 0.01$ and $L = 10$) appears to be very close to the ZND-based model prediction, at least for $20 \leq E_{\text{a}} \leq 40$. This remarkably good agreement suggests that, in near-limit scenarios, there may be some effective similarity between the detonation dynamics arising from a highly inhomogeneous medium and that considered in the ZND-based model. Considering a case with spatially highly discretized reactive sources, the chemical energy of the medium is concentrated into very small regions. The dimensionless energy density within a discrete source is Q/Γ while that of a homogeneous medium is Q. For the same activation energy and shock strength, the amount of energy released in the concentrated source is proportionally greater than that of the reactant in a homogenous medium. The greater energy release results in a greater local temperature at

this source, which further accelerates the rate of energy release from the source. Due to this positive-feedback mechanism, the amount of gas that reacts slowly in the homogeneous medium case is significantly reduced in the inhomogeneous cases or completely eliminated in the limit of $\Gamma \to 0$. Thus, the energy release of discrete sources is likely more coherent with the leading shock complex, which is effectively similar to the scenario pictured by the ZND-based model, wherein the energy release zone is closely attached to the leading shock. This effective similarity might provide an explanation for why a smooth-curvature-based model can fairly well capture the macroscopic dynamics of detonations in condensed-phase explosives that are sensitized by mesoscale inhomogeneities, e.g., the DSD model for detonation in ammonium nitrate/fuel oil (ANFO) [61].

In the limit of large activation energy, a parcel of shocked reactant tends to undergo an effective induction process with minimal amount of energy release. The positive-feedback energy release mechanism of highly discretized sources (as elucidated in the previous paragraph) may shorten the duration of this effective induction process. This effect is likely suggested by the fact that, for $E_\mathrm{a} = 55$, the critical thickness resulting from the highly inhomogeneous case is considerably thinner than the ZND-based model prediction (as shown in Fig. 8). The intense energy release of these discrete sources governed by highly activated kinetics may share some similarity with the strong, localized explosions that have been experimentally observed and conjectured to dominate the critical phenomena in highly unstable gaseous detonations [62].

By performing numerical convergence tests for selected cases in this study, it has been found that the simulations with the discretized sources can be more easily converged numerically than the simulations of homogeneous media (see Appendix). Relatively modest computational resolutions (five computational cells per half-reaction-zone length of the ZND solution for the homogeneous case, i.e., $l_{1/2}/\Delta x = 5$) were able to identify the critical layer thickness that was confirmed as the resolution was increased to as great as $l_{1/2}/\Delta x = 30$. This resolution was not sufficient to resolve the reaction zone structure inside the reactive pockets, but resolving these features may not be necessary to capture the overall dynamics of the wave. This behavior is quite different from that in homogeneous simulations, wherein the critical layer thickness continued to vary (increase) as the numerical resolution was increased to $l_{1/2}/\Delta x = 30$. In fact, converged simulations were not possible at activation energies greater than $E_\mathrm{a} = 30$ with current computational resources. The result might indicate that the discrete source approach may be a way to explore the dynamics of detonations governed by high activation energies ($E_\mathrm{a} > 50$) representative of real hydrocarbon mixtures.

6 Conclusion

The results of this study have demonstrated that concentrating the energy release of a medium into spatially concentrated sources—leaving inert gas in-between the sources with the overall energy release of the media remaining the same—results in a detonation wave that is able to propagate in significantly thinner layers. This effect becomes more significant as activation energy is increased, with the difference between the critical layer thickness and a homogenous reactive layer and a highly inhomogeneous layer ($\Gamma = 0.01$) being as much as a factor of five times different. For sufficiently low activation energy ($E_\mathrm{a} \to 10$), laminar-like propagation is still possible, and under these conditions, the simulations in the homogenous media and the discretized media converge and are in good agreement with a simple front-curvature based model deriving from the classic work of Wood and Kirkwood.

In the case of highly discretized sources, the critical layer thickness is in remarkably good agreement with the predictions of the classic Wood and Kirkwood model based upon front curvature over the range of activation energies studied, particularly over the range $10 < E_\mathrm{a} < 40$. This surprising result, in which a highly heterogeneous media results in detonation dynamics that is in better agreement with a ZND-based model than detonation in a perfectly homogeneous media, is reminiscent of polycrystalline explosives. In condensed phase explosives, hot spots reduce the sensitivity to the bulk temperature of the shock-compressed media and effectively "wash out" the inherent instabilities, resulting in an effectively laminar-like structure governed by average front curvature.

Another finding in this study is the easiness (i.e., coarser resolutions that are necessary) to obtain numerically converged results of critical thickness for the highly inhomogeneous cases. Although it was very difficult to obtain numerical convergence for the simulations with $E_\mathrm{a} > 30$ and homogeneous media, fully converged results of critical thickness were obtained at relatively low resolutions for the cases with highly discretized sources governed by very large activation energies (e.g., $E_\mathrm{a} = 55$).

Appendix: Numerical convergence study

For two selected values of moderately high activation energy considered, i.e., $E_a = 20$ and $E_a = 30$, numerical convergence tests were performed for the homogeneous cases ($\Gamma = 1$) and the most highly discretized cases ($\Gamma = 0.01$ and $L = 10$). The convergence study for the resulting critical reactive layer thickness h^* from these cases is shown as the "go" vs. "no-go" charts plotted in Figs. 9 and 10.

In Figs. 9, 10, and 11, each symbol represents a case of one or several simulations with a reactive layer thickness h at a numerical resolution in terms of the number of computational cells per the ideal half-reaction-zone length $l_{1/2}/\Delta x$. In these figures, a circle $\circ$ indicates a "go", i.e., a case resulting in a self-sustainable propagation; a cross $\times$ indicates a "no-go", i.e., a case of propagation failure. The dashed line indicates the boundary between "go" and "no-go" results that defines the critical thickness h^* as a function of numerical resolution. Considering the stochastic nature of the distribution of reactive sources in a highly inhomogeneous medium, for the near-limit cases, five simulations have been performed for the same value of h. Only if all of these five simulations result in a successful wave propagation over a distance that is more than approximately 150 times the average source spacing L, the case with the corresponding h is considered as a "go".

For the homogeneous case with $E_a = 20$ shown in Fig. 9(a), as the numerical resolution was increased from $l_{1/2}/\Delta x = 10$ to 20, the result of h^* increased by approximately 9%. As the numerical resolution was increases from $l_{1/2}/\Delta x = 20$ to 30, there was no change greater than $\pm 4\%$ in the result of h^*. For the highly discretized case with $E_a = 20$, $\Gamma = 0.01$, and $L = 10$ shown in Fig. 9(b), there was no change greater than the prescribed average source spacing L in the result of h^* as the resolution was increased from $l_{1/2}/\Delta x = 5$ to 30. For $E_a = 30$, the homogeneous case shown in Fig. 10(a), as the numerical resolution was increased from $l_{1/2}/\Delta x = 5$ to 10, the result of h^* increased by approximately 26%. As the numerical resolution was increased from $l_{1/2}/\Delta x = 10$ to 20, the change in the result of h^* was less than $\pm 1\%$. As shown in Fig. 10(b) for the highly discretized case with $E_a = 30$, $\Gamma = 0.01$, and $L = 10$, there was no change greater than the prescribed average source spacing L in the result of h^* as the resolution was increased from $l_{1/2}/\Delta x = 5$ to 20.

For the homogeneous cases with both $E_a = 20$ and $E_a = 30$ as shown in Figs. 9(a) and 10(a), respectively, simulations at a relatively coarse resolution result in a smaller critical thickness. This reduction in h^* could be attributed to the fact that the effect of numerical diffusion becomes more significant when the inviscid Euler equations are solved at coarser resolutions. In a cellular detonation structure that arises from a homogeneous reactive medium, there is a large amount of reactant that is shocked by the weak parts of the leading shock and undergoes a very slow burning process. The efficiency of this slow reaction process can be significantly enhanced by numerical diffusion. Simulations at coarse resolution likely result in an artificially (numerically) enhanced energy release rate and, thus, enables a detonation wave to propagate in a thinner reactive layer.

For the large values of activation energy $E_a = 40$ and 55, the simulations have been performed only for the highly inhomogeneous cases with $\Gamma = 0.01$ and $L = 10$. As shown in Fig. 11(a) for the cases with $E_a = 40$, simulations at three different resolutions $l_{1/2}/\Delta x = 10$, 20, and 30 resulted in the same critical thickness. For the cases with the greatest value of activation energy considered in this study $E_a = 55$, a minimal resolution of $l_{1/2}/\Delta x = 20$ was required to obtain numerically converged result of h^* as shown in Fig. 11(b). Therefore, the results of h^* as a function of E_a presented in Fig. 8 were all based on the simulations at a resolution of $l_{1/2}/\Delta x = 10$ except the data point for the $E_a = 55$, highly inhomogeneous case, which was performed at a resolution of $l_{1/2}/\Delta x = 20$.

Acknowledgements The authors thank M. Radulescu, A. Chinnayya, M. Reynaud, and S. Taileb for valuable discussions and critiques of this work. The Tesla K40M processors were acquired under Nvidia's GPU Grant Program. The Tesla P100 GPU resources were provided by Compute Canada.

References

1. W. Wood, J. Kirkwood, Diameter effect in condensed explosives. The relation between velocity and radius of curvature of the detonation wave, The Journal of Chemical Physics **22**(11), 1920 (1954). DOI 10.1063/1.1739940
2. J. Fay, Two-dimensional gaseous detonations: Velocity deficit, The Physics of Fluids **2**(3), 283 (1959). DOI 10.1063/1.1705924
3. W. Fickett, W. Davis, *Detonation: Theory and Experiment* (Dover Publications, 1979)
4. A. Higgins, Steady one-dimensional detonations, in *Shock Waves Science and Technology Library*, vol. 6, ed. by F. Zhang (Springer Berlin Heidelberg, 2012), pp. 33–105. DOI 10.1007/978-3-642-22967-1_2
5. M. Radulescu, J. Lee, The failure mechanism of gaseous detonations: experiments in porous wall tubes, Combustion and Flame **131**(12), 29 (2002). DOI 10.1016/S0010-2180(02)00390-5
6. M. Radulescu, The propagation and failure mechanism of gaseous detonations : experiments in porous-walled tubes. Ph.D. thesis, McGill University (2003)
7. B. Borzou, M. Radulescu, Dynamics of detonations with a constant mean flow divergence, arXiv preprint arXiv:1606.05323 (2016)

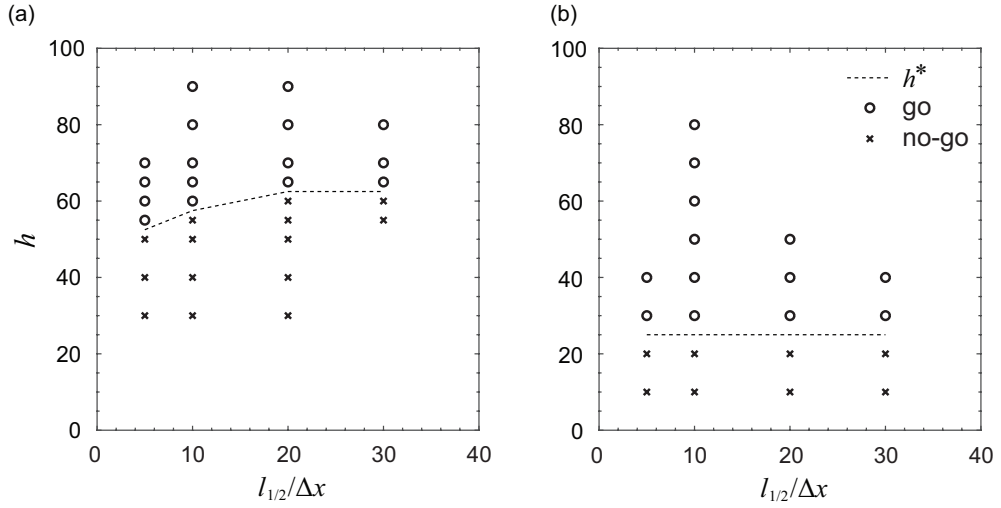

Fig. 9 Numerical convergence study for the result of critical reactive layer thickness h^* with $E_a = 20$ for (a) homogeneous cases and (b) inhomogeneous cases with $\Gamma = 0.01$ and $L = 10$.

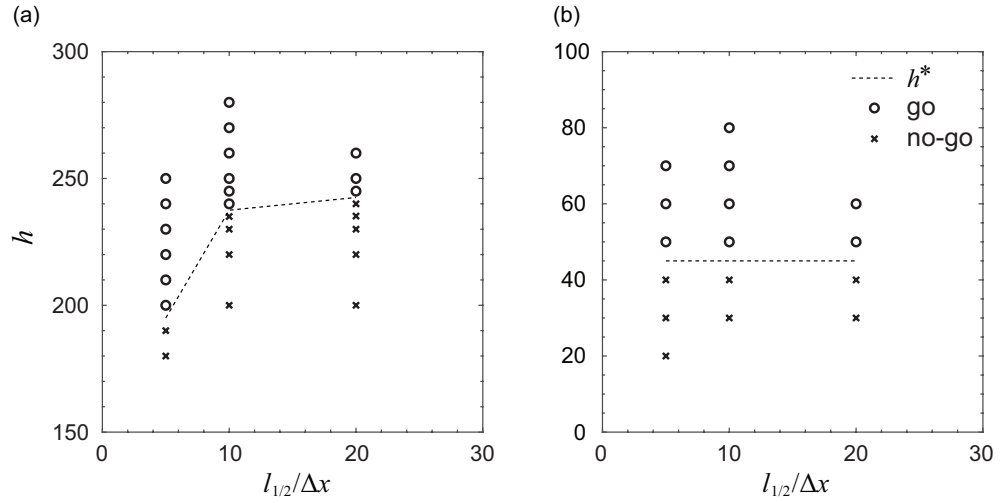

Fig. 10 Numerical convergence study for the result of critical reactive layer thickness h^* with $E_a = 30$ for (a) homogeneous cases and (b) inhomogeneous cases with $\Gamma = 0.01$ and $L = 10$.

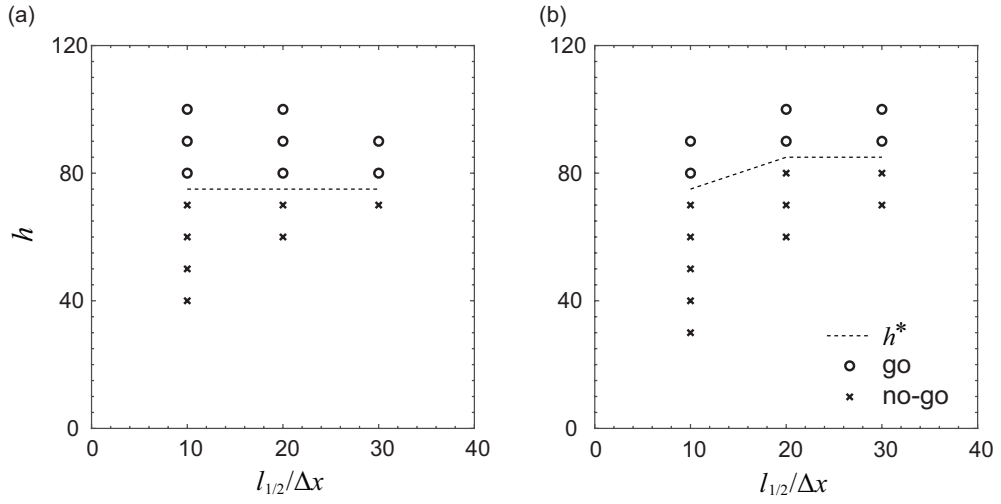

Fig. 11 Numerical convergence study for the result of critical reactive layer thickness h^* with an inhomogeneous medium with $\Gamma = 0.01$ and $L = 10$ for (a) $E_a = 40$ and (b) $E_a = 55$.

8. E. Oran, J. Boris, T. Young, M. Flanigan, T. Burks, M. Picone, Numerical simulations of detonations in hydrogen-air and methane-air mixtures, Symposium (International) on Combustion **18**(1), 1641 (1981). DOI 10.1016/S0082-0784(81)80168-3
9. E. Oran, T. Young, J. Boris, J. Picone, D. Edwards, A study of detonation structure: The formation of unreacted gas pockets, Symposium (International) on Combustion **19**(1), 573 (1982). DOI 10.1016/S0082-0784(82)80231-2
10. M. Reynaud, F. Virot, A. Chinnayya, A computational study of the interaction of gaseous detonations with a compressible layer, Physics of Fluids **29**(5), 056101 (2017). DOI 10.1063/1.4982659
11. M. Reynaud, Numerical Study of Detonation Confined by an Inert Gas. Theses, ISAE-ENSMA École Nationale Supérieure de Mécanique et d'Aérotechique - Poitiers (2017)
12. M. Radulescu, G. Sharpe, J. Lee, C. Kiyanda, A. Higgins, R. Hanson, The ignition mechanism in irregular structure gaseous detonations, Proceedings of the Combustion Institute **30**(2), 1859 (2005). DOI http://dx.doi.org/10.1016/j.proci.2004.08.047
13. M. Radulescu, G. Sharpe, C. Law, J. Lee, The hydrodynamic structure of unstable cellular detonations, Journal of Fluid Mechanics **580**, 31 (2007). DOI 10.1017/S0022112007005046
14. B. Maxwell, R. Bhattacharjee, S. Lau-Chapdelaine, S. Falle, G. Sharpe, M. Radulescu, Influence of turbulent fluctuations on detonation propagation, Journal of Fluid Mechanics **818**, 646 (2017). DOI 10.1017/jfm.2017.145
15. F. Pintgen, C. Eckett, J. Austin, J. Shepherd, Direct observations of reaction zone structure in propagating detonations, Combustion and Flame **133**(3), 211 (2003). DOI 10.1016/S0010-2180(02)00458-3
16. J. Austin, F. Pintgen, J. Shepherd, Reaction zones in highly unstable detonations, Proceedings of the Combustion Institute **30**(2), 1849 (2005). DOI 10.1016/j.proci.2004.08.157
17. J. Shepherd, Detonation in gases, Proceedings of the Combustion Institute **32**(1), 83 (2009). DOI 10.1016/j.proci.2008.08.006
18. C. Kiyanda, A. Higgins, Photographic investigation into the mechanism of combustion in irregular detonation waves, Shock Waves **23**(2), 115 (2013). DOI 10.1007/s00193-012-0413-8
19. X. Mi, A. Higgins, Influence of discrete sources on detonation propagation in a Burgers equation analog system, Physical Review E **91**, 053014 (2015). DOI 10.1103/PhysRevE.91.053014
20. X. Mi, E. Timofeev, A. Higgins, Effect of spatial discretization of energy on detonation wave propagation, Journal of Fluid Mechanics **817**, 306 (2017). DOI 10.1017/jfm.2017.81
21. X. Mi, A. Higgins, H. Ng, C. Kiyanda, N. Nikiforakis, Propagation of gaseous detonation waves in a spatially inhomogeneous reactive medium, Physical Review Fluids **2**(5), 053201 (2017). DOI 10.1103/PhysRevFluids.2.053201
22. X. Mi, Detonation in spatially inhomogeneous media. Ph.D. thesis, McGill University (2018)
23. W. Sommers, R. Morrison, Simulation of condensed-explosive detonation phenomena with gases, Phys. Fluids **5**(3), 241 (1962). DOI 10.1063/1.1706602
24. E. Dabora, J. Nicholls, R. Morrison, The influence of a compressible boundary on the propagation of gaseous detonations, Symposium (International) on Combustion **10**(1), 817 (1965). DOI 10.1016/S0082-0784(65)80225-9
25. E. Dabora, J. Nicholls, M. Sichel, The interaction process between gaseous detonation waves and inert gaseous boundaries: final report. Tech. Rep. 05170-3-F, The University of Michigan, Aircraft Propulsion Laboratory (1965)
26. S. Murray, J. Lee, The influence of yielding confinement on large-scale ethylene-air detonations, Prog. Astronaut. Aeronaut **94**, 80 (1984). DOI 10.2514/5.9781600865695.0080.0103
27. S. Murray, J. Lee, The influence of physical boundaries on gaseous detonation waves, Prog. Astronaut. Aeronaut **106**, 329 (1986). DOI 10.2514/5.9781600865800.0329.0355
28. A. Vasil'ev, D. Zak, Detonation of gas jets, Comb. Expl. Shock **22**, 463 (1986). DOI 10.1007/BF00862893
29. A. Borisov, S. Khomic, V. Mikhalkin, Detonation of unconfined and semiconfined charges of gaseous mixtures, Prog. Astronaut. Aeronaut **133**, 118 (1991). DOI 10.2514/5.9781600866067.0118.0132
30. W. Rudy, M. Kuznetsov, R. Porowski, A. Teodorczyk, J. Grune, K. Sempert, Critical conditions of hydrogen-air detonation in partially confined geometry, Proceedings of the Combustion Institute **34**(2), 1965 (2013). DOI 10.1016/j.proci.2012.07.019
31. W. Rudy, M. Zbikowski, A. Teodorczyk, Detonations in hydrogen-methane-air mixtures in semi confined flat channels, Energy **116**, 1479 (2016). DOI 10.1016/j.energy.2016.06.001
32. W. Rudy, K. Dziubanii, M. Zbikowski, A. Teodorczyk, Experimental determination of critical conditions for hydrogen-air detonation propagation in partially confined geometry, International Journal of Hydrogen Energy **42**(11), 7366 (2017). DOI 10.1016/j.ijhydene.2016.04.056
33. J. Grune, K. Sempert, A. Friedrich, M. Kuznetsov, T. Jordan, Detonation wave propagation in semi-confined layers of hydrogen–air and hydrogen–oxygen mixtures, International Journal of Hydrogen Energy **42**(11), 7589 (2017). DOI 10.1016/j.ijhydene.2016.06.055
34. R. Houim, R. Fievisohn, The influence of acoustic impedance on gaseous layered detonations bounded by an inert gas, Combustion and Flame **179**, 185 (2017). DOI 10.1016/j.combustflame.2017.02.001
35. A. Gaathaug, K. Vaagsaether, D. Bjerketvedt, in *26^{th} International Colloquium on the Dynamics of Explosions and Reactive Systems* (2017), 908. Boston, MA
36. K. Cho, J. Codoni, B. Rankin, J. Hoke, F. Schauer, in *55^{th} AIAA Aerospace Sciences Meeting* (2017), 0373. DOI 10.2514/6.2017-0373. Grapevine, TX
37. J. Burr, K. Yu, in *53^{rd} AIAA/SAE/ASEE Joint Propulsion Conference* (2017), 4908. DOI 10.2514/6.2017-4908. Atlanta,GA
38. J. Fujii, Y. Kumazawa, A. Matsuo, S. Nakagami, K. Matsuoka, J. Kasahara, Numerical investigation on detonation velocity in rotating detonation engine chamber, Proceedings of the Combustion Institute **36**(2), 2665 (2017). DOI 10.1016/j.proci.2016.06.155
39. N. Ohira, A. Matsuo, J. Kasahara, K. Matsuoka, in *26^{th} International Colloquium on the Dynamics of Explosions and Reactive Systems* (2017), 994. Boston, MA
40. E.F. Toro, *Riemann Solvers and Numerical Methods for Fluid Dynamics*, 3rd edn. (Springer, 2009). DOI 10.1007/978-3-662-03490-3
41. G. Morgan, The Euler equations with a single-step Arrhenius reaction. Master's thesis, University of Cambridge (2013)

42. C. Kiyanda, G. Morgan, N. Nikiforakis, H. Ng, High resolution gpu-based flow simulation of the gaseous methane-oxygen detonation structure, Journal of Visualization **18**(2), 273 (2015). DOI 10.1007/s12650-014-0247-9
43. J. Li, X. Mi, A. Higgins, in 15^{th} *Symposium (International) on Detonation* (Office of Naval Research, Arlington, 2014)
44. J. Li, X. Mi, A. Higgins, Effect of spatial heterogeneity on near-limit propagation of a pressure-dependent detonation, Proceedings of the Combustion Institute **35**(2), 2025 (2015). DOI 10.1016/j.proci.2014.06.039
45. J. Li, X. Mi, A. Higgins, Geometric scaling for a detonation wave governed by a pressure-dependent reaction rate and yielding confinement, Physics of Fluids **27**(2), 027102 (2015). DOI 10.1063/1.4907267
46. E. Oran, J. Boris, *Numerical simulation of reactive flow* (Cambridge University Press, 2005)
47. A. Kasimov, D. Stewart, On the dynamics of self-sustained one-dimensional detonations: A numerical study in the shock-attached frame, Physics of Fluids **16**(10), 3566 (2004)
48. A. Bourlioux, A. Majda, Theoretical and numerical structure for unstable two-dimensional detonations, Combustion and Flame **90**(3), 211 (1992). DOI 10.1016/0010-2180(92)90084-3
49. G. Sharpe, Linear stability of idealized detonations, Proceedings of the Royal Society of London A: Mathematical, Physical and Engineering Sciences **453**(1967), 2603 (1997)
50. M. Short, D. Stewart, Cellular detonation stability: A normal mode linear analysis, Journal of Fluid Mechanics **368**, 229 (1998)
51. G. Sharpe, S. Falle, One-dimensional numerical simulations of idealized detonations, Proceedings of the Royal Society of London A: Mathematical, Physical and Engineering Sciences **455**(1983), 1203 (1999)
52. P. Hwang, R. Fedkiw, B. Merriman, T. Aslam, A. Karagozian, S. Osher, Numerical resolution of pulsating detonation waves, Combustion Theory and Modelling **4**(3), 217 (2000). DOI 10.1088/1364-7830/4/3/301
53. G. SHARPE, Transverse waves in numerical simulations of cellular detonations, Journal of Fluid Mechanics **447**, 3151 (2001). DOI 10.1017/S0022112001005535
54. H. Ng, A. Higgins, C. Kiyanda, M. Radulescu, J. Lee, K. Bates, N. Nikiforakis, Nonlinear dynamics and chaos analysis of one-dimensional pulsating detonations, Combustion Theory and Modelling **9**(1), 159 (2005). DOI 10.1080/13647830500098357
55. A. Henrick, T. Aslam, J. Powers, Simulations of pulsating one-dimensional detonations with true fifth order accuracy, Journal of Computational Physics **213**(1), 311 (2006). DOI http://dx.doi.org/10.1016/j.jcp.2005.08.013
56. H. Ng, F. Zhang, Detonation instability, in *Shock Waves Science and Technology Library*, vol. 6 (Springer Berlin Heidelberg, 2012), pp. 107–212
57. H. Eyring, R. Powell, G. Duffy, R. Parlin, The stability of detonation, Chemical Reviews **45**(1), 69 (1949). DOI 10.1021/cr60140a002
58. J. Bdzil, Steady-state two-dimensional detonation, Journal of Fluid Mechanics **108**, 195 (1981). DOI 10.1017/S0022112081002085
59. J. Bdzil, D. Stewart, Modeling two-dimensional detonations with detonation shock dynamics, Physics of Fluids A: Fluid Dynamics (1989-1993) **1**(7), 1261 (1989). DOI 10.1063/1.857349
60. J. Bdzil, D. Stewart, Theory of detonation shock dynamics, in *Shock Waves Science and Technology Library*, vol. 6 (Springer Berlin Heidelberg, 2012), pp. 373–453. DOI 10.1007/978-3-642-22967-1_7
61. J. Bdzil, T. Aslam, R. Catanach, L. Hill, M. Short, Dsd front models: nonideal explosive detonation in anfo. Tech. rep., Los Alamos National Laboratory (2002)
62. J. Lee, On the critical tube diameter, in *Dynamics of Exothermicity*, ed. by J. Bowen (Gordon and Breach, Amsterdam, 1996), p. 321